Supporting Information

Atomically Precise Metal Nanoclusters Combine with MXene Towards Solar CO_2 Conversion

Yu-Shan Cai, [a] Jia-Qi Chen, [a] Peng Su, [a] Xian Yan, [a] Qing Chen, [a] Yue Wu, [a] Fang-Xing Xiao [*a, b]

a. College of Materials Science and Engineering, Fuzhou University, New Campus, Minhou, Fujian Province, 350108, China.

b. State Key Laboratory of Structural Chemistry, Fujian Institute of Research on the Structure of Matter, Chinese Academy of Sciences, Fuzhou, Fujian 350002, PR China.

E-mail: fxxiao@fzu.edu.cn

1. Experimental section

1.1 Materials

Cadmium chloride ($CdCl_2 \cdot 2.5H_2O$), Sulfur powder (S), hydrochloric acid (HCl), lithium fluoride (LiF), 2-mercaptoethylamine (MEA), Au_x clusters Gold (III) chloride trihydrate ($HAuCl_4 \cdot 3H_2O$), ethanol (C_2H_6O, EtOH), acetonitrile (C_2H_3N), triethanolamine ($C_6H_{15}NO_3$, TEOA), DL-Lactic acid ($C_3H_6O_3$), Methanol (CH_4O), Ethanol (C_2H_6O), Ethylene glycol ($C_2H_6O_2$) and sodium sulfate (Na_2SO_4) were obtained from Sinopharm Chemical Reagent Co., Ltd. (Shanghai, China). Ti_3AlC_2 power was obtained from Laizhou Kai Kai Ceramic Materials Co., Ltd. L-glutathione (GSH) was obtained from Sigma-Aldrich.Deionized water (DI H_2O, Millipore,18.2 MΩ·cm resistivity).

1.2 Photoelectrochemical (PEC) measurements

PEC measurements were carried out on electrochemical workstations (CHI 660E and Gamary Interface 1000 E) in a conventional three-electrode quartz cell, which use Pt plate as the counter electrode, Ag/AgCl electrode as the reference electrode, and the samples coated on FTO were utilized as the working electrodes. The working electrodes were prepared on fluorine-dope tin oxide (FTO) glass that was cleaned by sonication in ethanol for 30 min and dried at 353 K. The boundary of FTO glass was protected using scotch tape. The 5 mg sample was completely dispersed in 0.5 mL of ethyl alcohol absolute by sonication to get slurry which uniformly was spread onto the pretreated FTO glass. After drying in the air, the working electrode was further dried at 353 K for 2 h to improve adhesion. Then the Scotch tape was unstuck, and the uncoated part of the electrode was isolated with nail polish. The exposed area of the working electrode was 1 cm^2. Besides, Na_2SO_4 (0.5 M, pH=6.69) aqueous solution was used as the electrolyte. Average electron lifetime (τn) of the photoelectrode is determined by the following equation:

$$\tau = \frac{k_B T}{e(dV_{oc}/dt)^{-1}} \qquad \text{Equation (1)}$$

where τ is the potential-dependent electron lifetime, k_B is the Boltzmann's constant (1.38×10^{-23} J/K), T is the temperature (298 K), e is the charge of a single electron (1.6×10^{-19} C), and V_{oc} is the open-circuit voltage

at time t. Charge carrier density (N_D) of photoelectrode is calculated by the formula below.

$$N_D = \left(\frac{2}{\varepsilon\varepsilon_0 e_0}\right)\left[\frac{d(1/c^2)}{dV}\right]^{-1} \qquad \text{Equation (2)}$$

where ε is the dielectric constant ($\varepsilon CdIn_2S_4$ =6.60), ε_0 is the vacuum permittivity (8.86×10^{-12} F/m), e_0 is the electronic charge unit (1.6×10^{-19} C), and V is the potential.

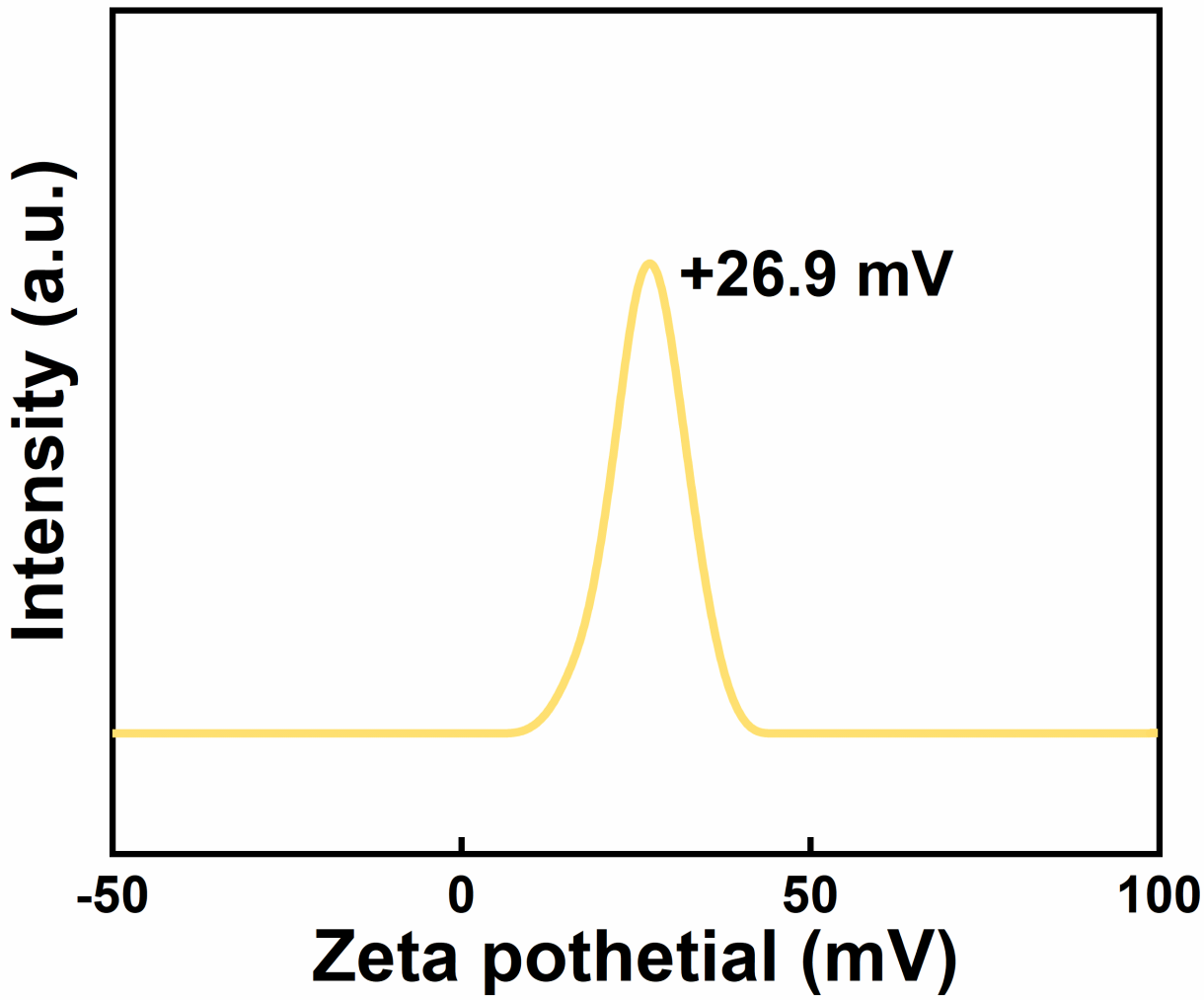

Fig. S1. Zeta potential of CdS aqueous solution.

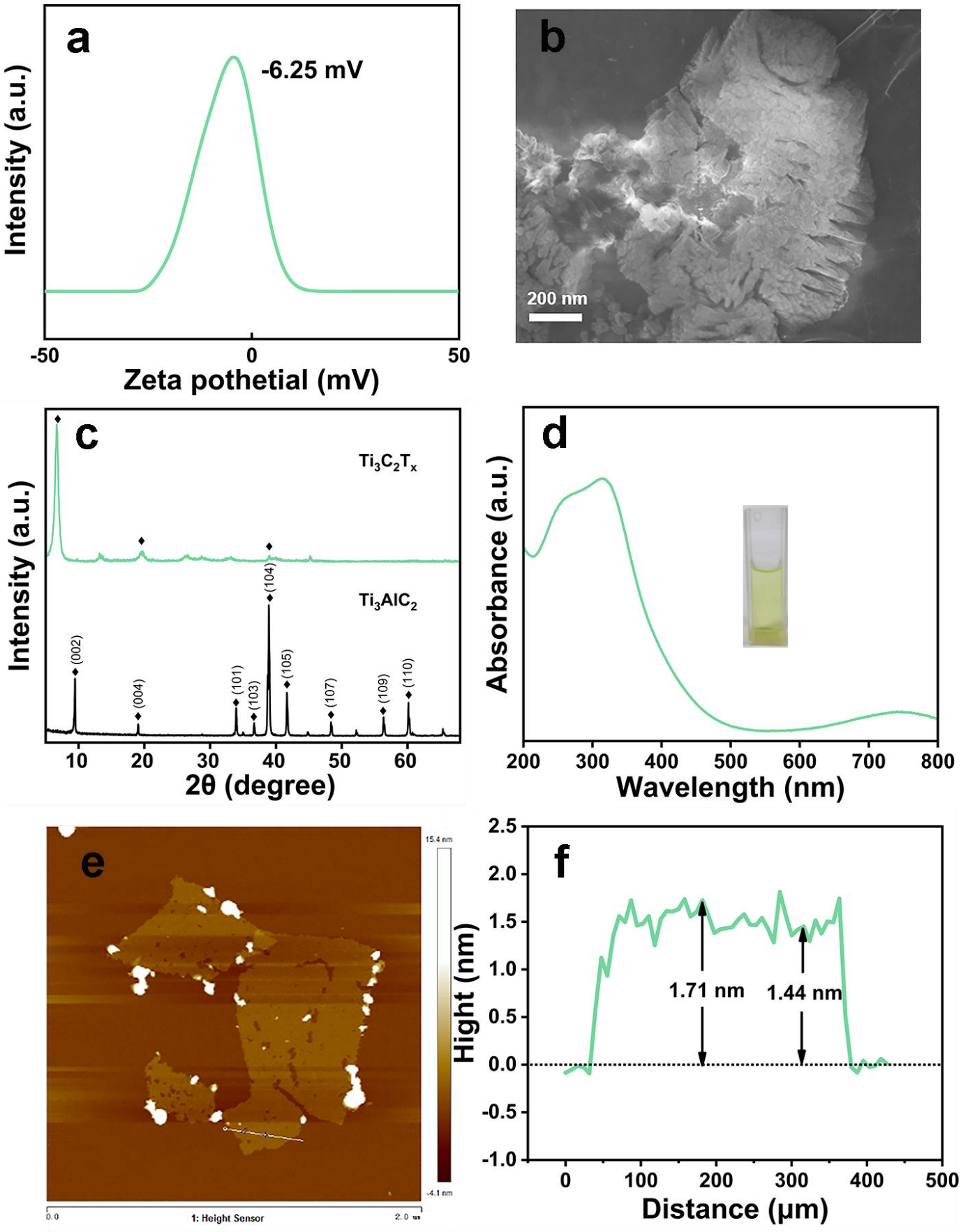

Fig. S2. (a) Zeta potential (pH=7), (b) FESEM image, (c) XRD pattern, (d) UV-vis absorption spectrum, (e) and AFM image & (f) height profile of $Ti_3C_2T_x$ NSs.

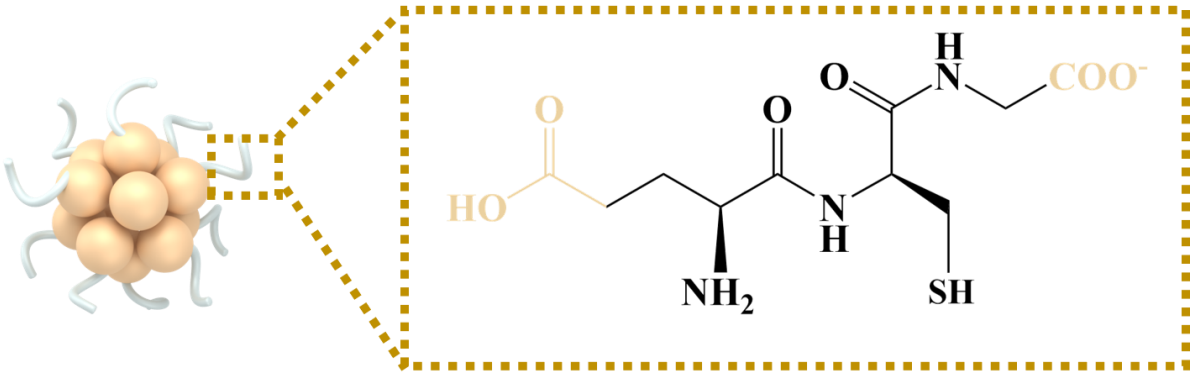

Fig. S3. Schematic model of Au_x NCs along with the molecular structure of GSH ligand.

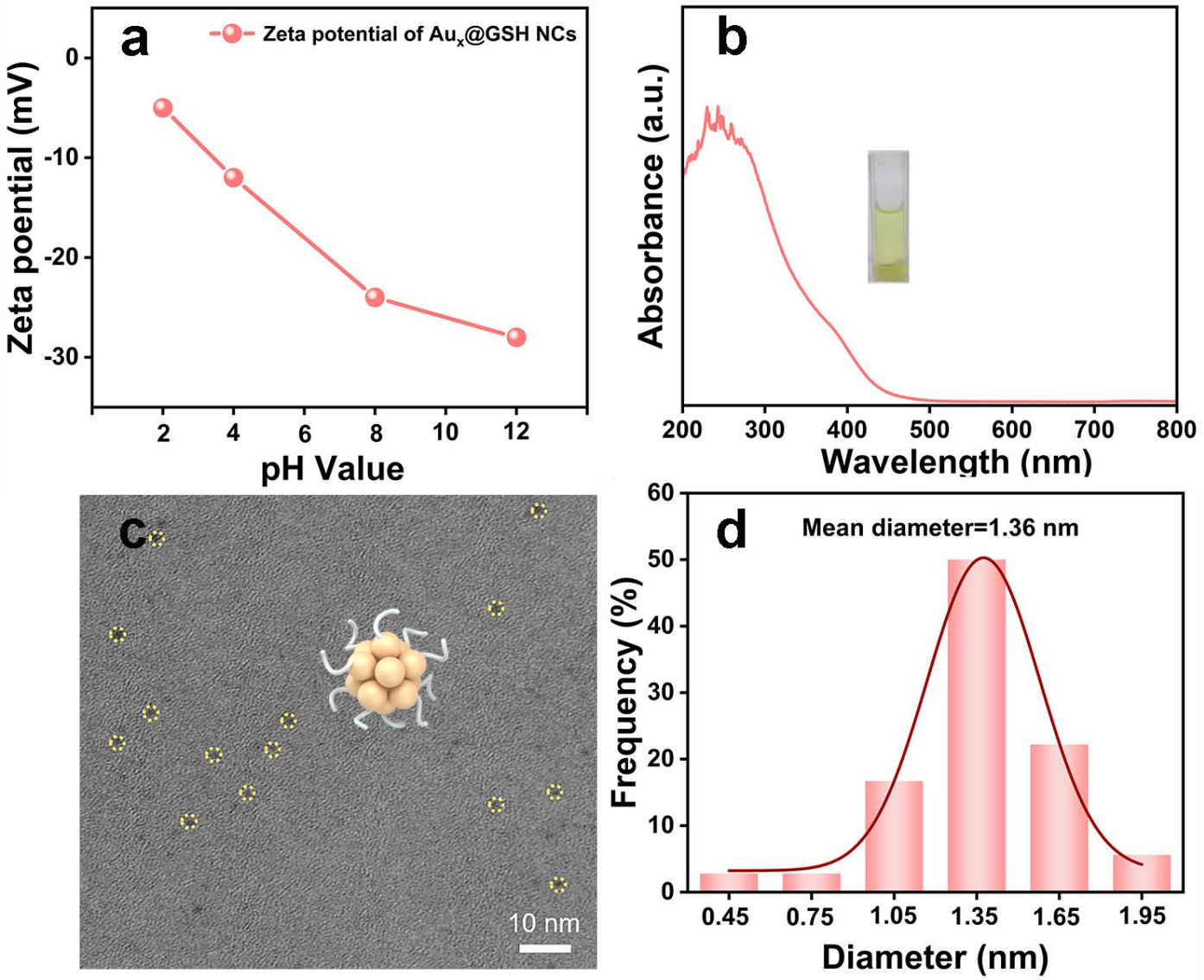

Fig. S4. (a) Zeta potentials and (b) UV-vis absorption spectrum, (c)TEM image and (d) size distribution histogram of Au_x@GSH NCs.

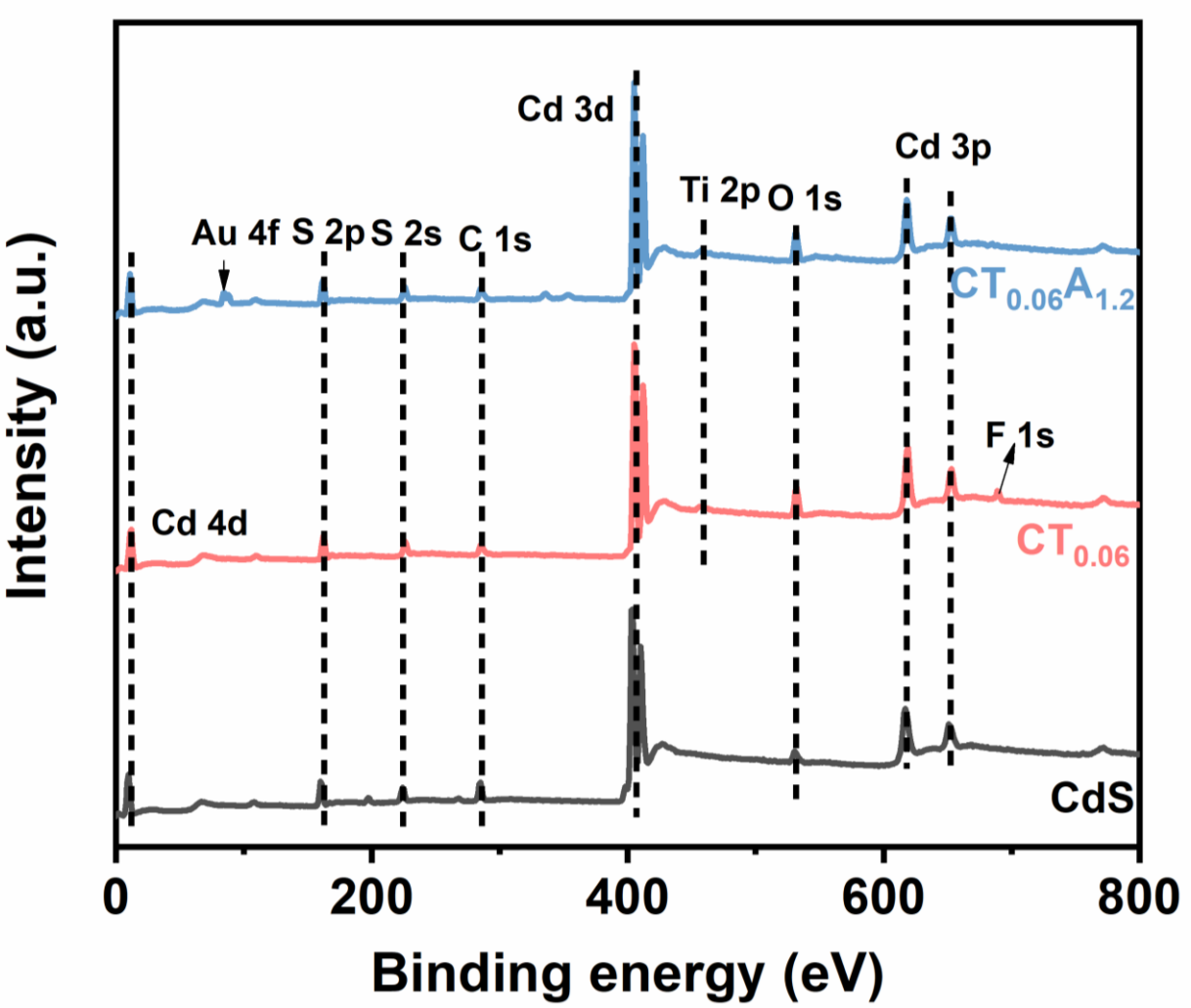

Fig. S5. Survey spectra of CdS, $CT_{0.06}$ and $CT_{0.06}A_{1.2}$.

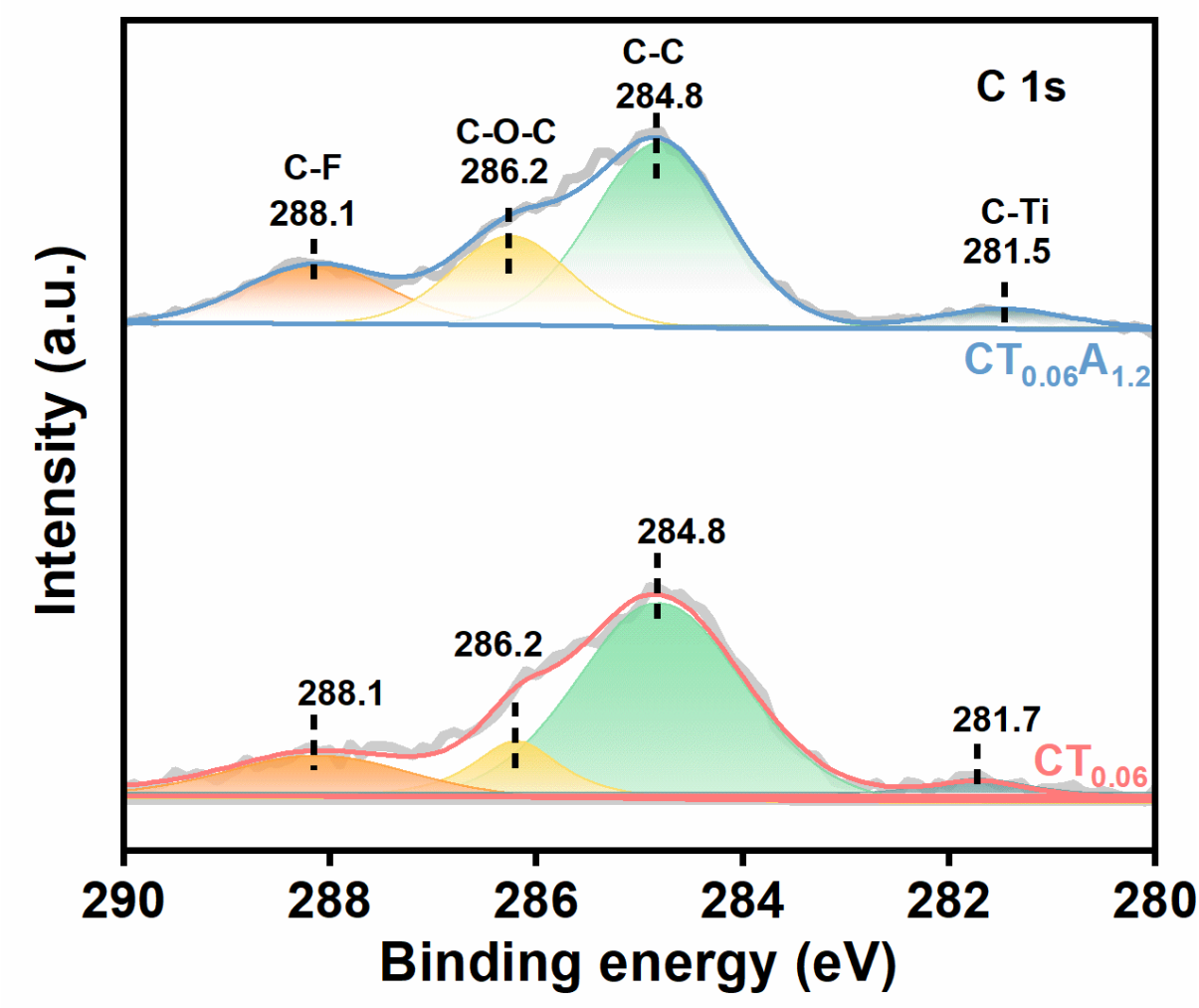

Fig. S6. High-resolution C 1s spectra of $CT_{0.06}$ and $CT_{0.06}A_{1.2}$.

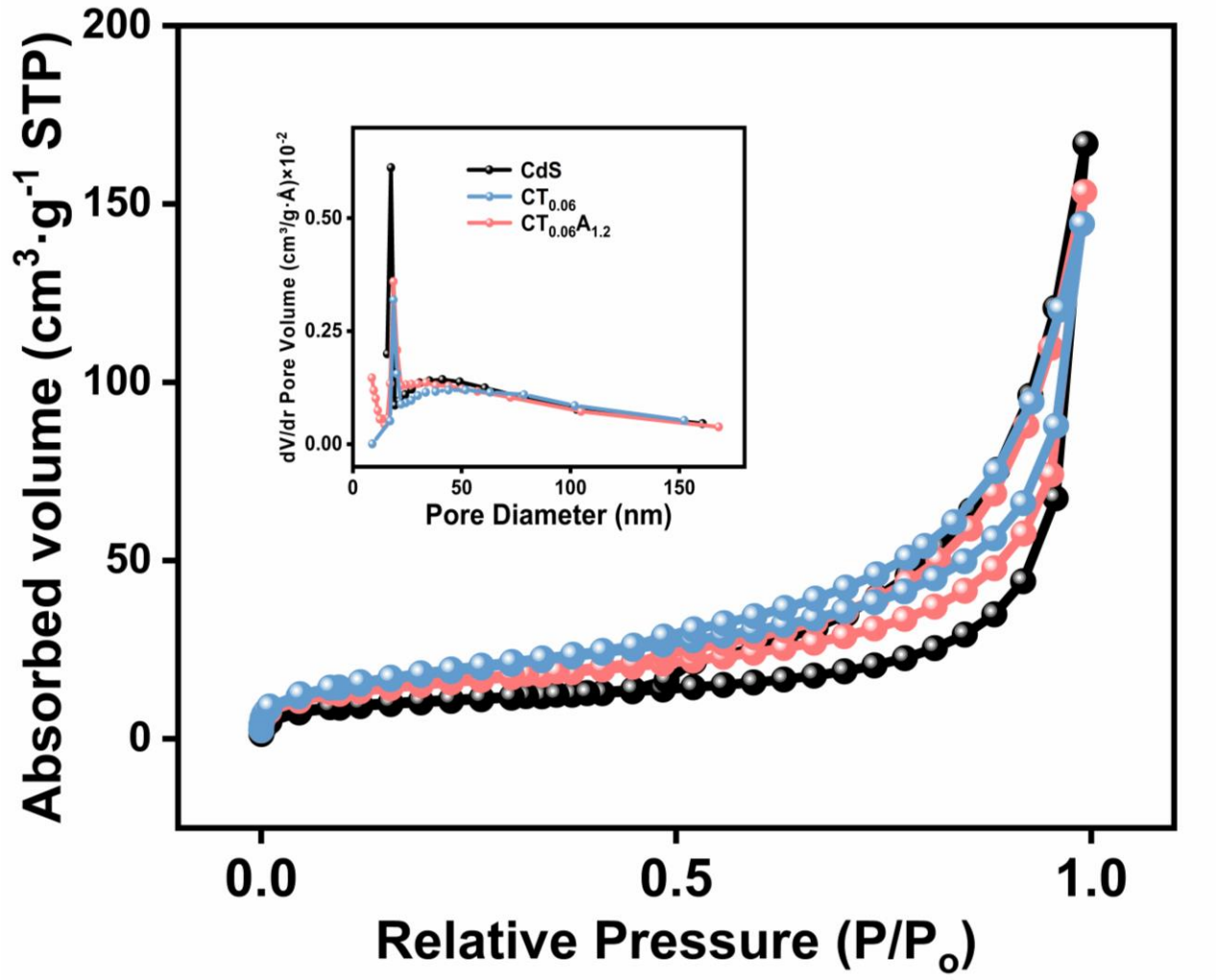

Fig. S7. Nitrogen adsorption/desorption isotherms and Pore-size distribution curves of CdS, $CT_{0.06}$ and $CT_{0.06}A_{1.2}$.

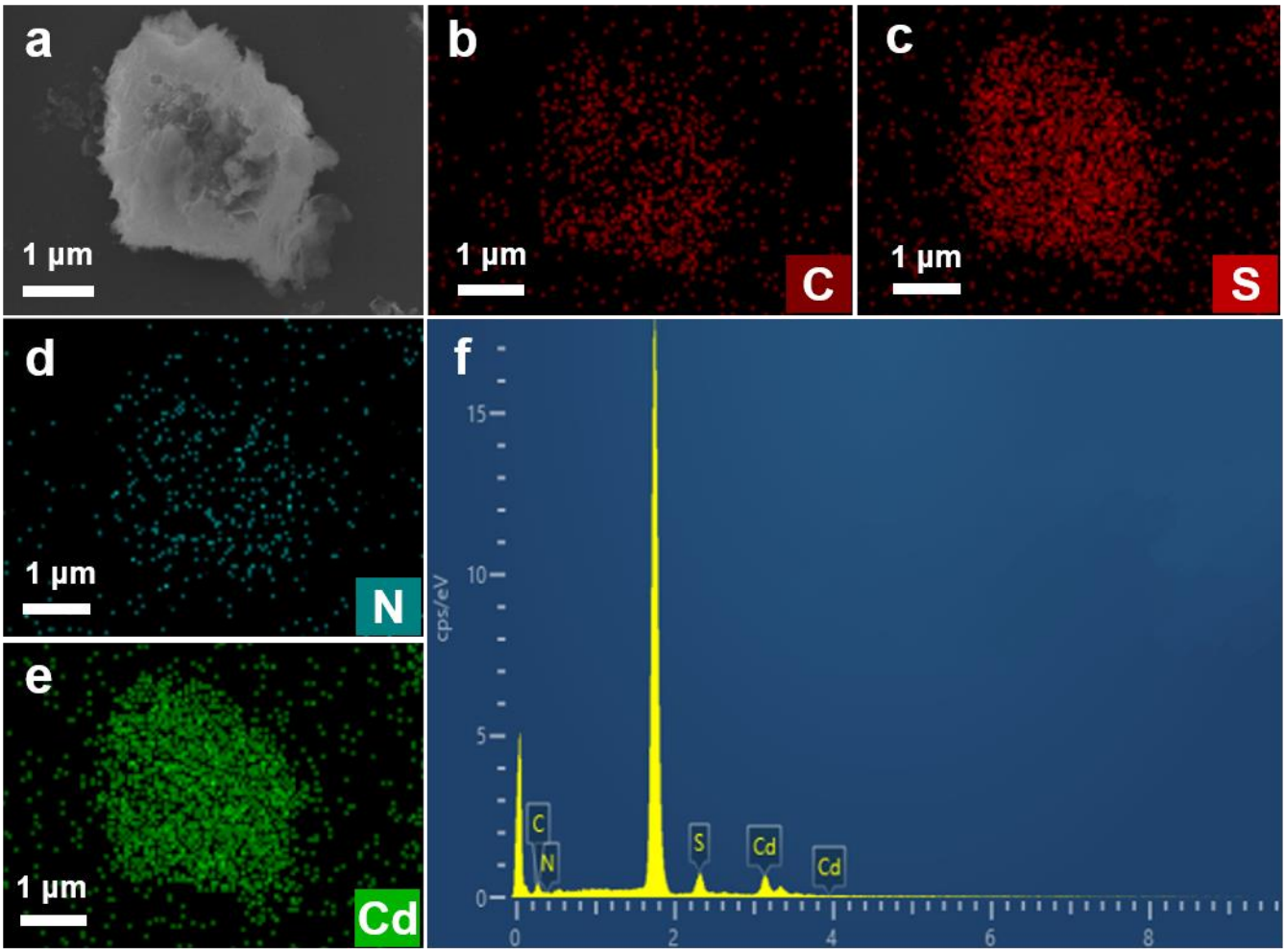

Fig. S8. (a) FESEM image and (b-e) elemental mapping & (f) EDS results of CdS NSs.

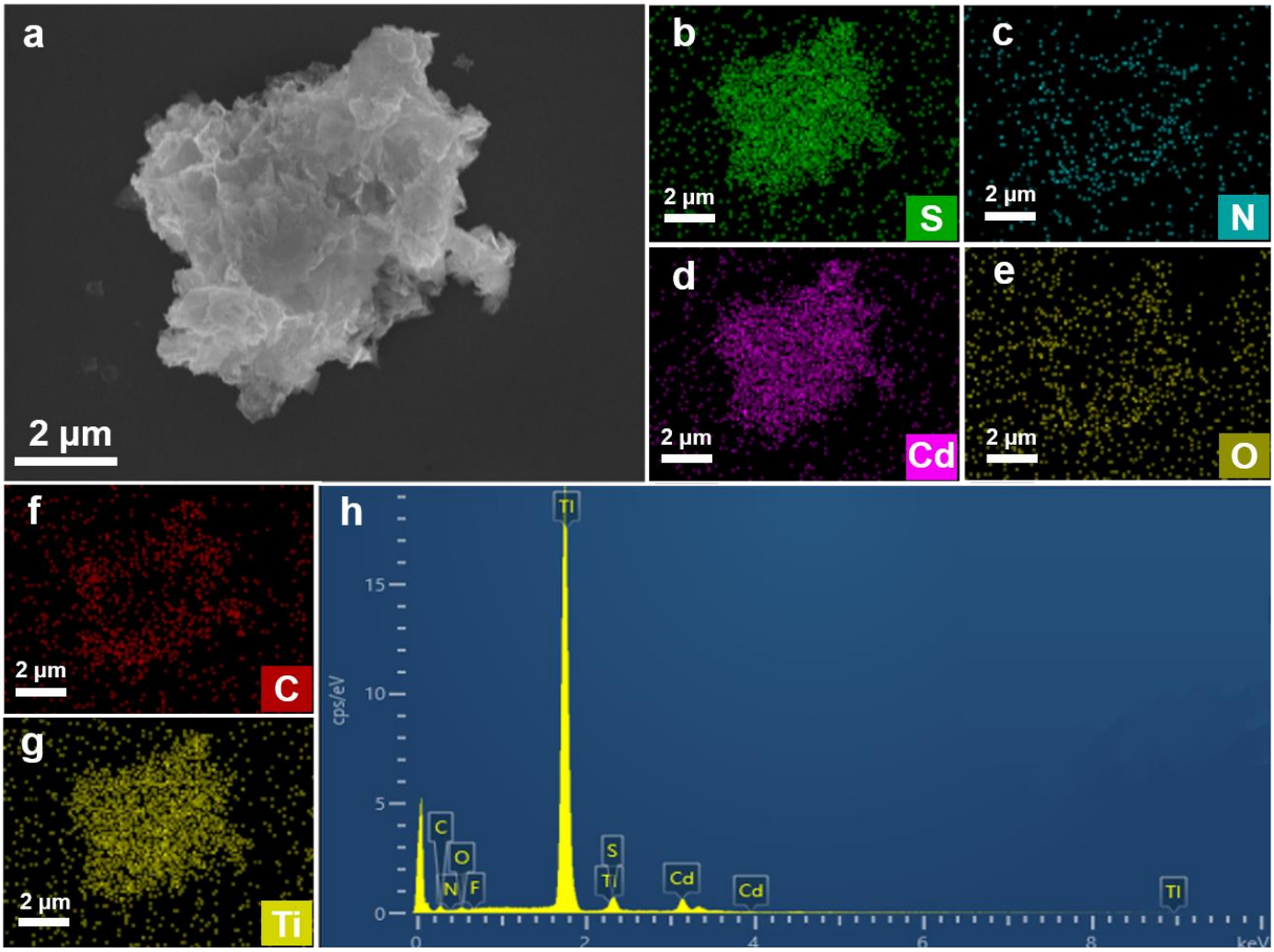

Fig. S9. (a) FESEM image and (b-g) elemental mapping & (h) EDS results of $CT_{0.06}$.

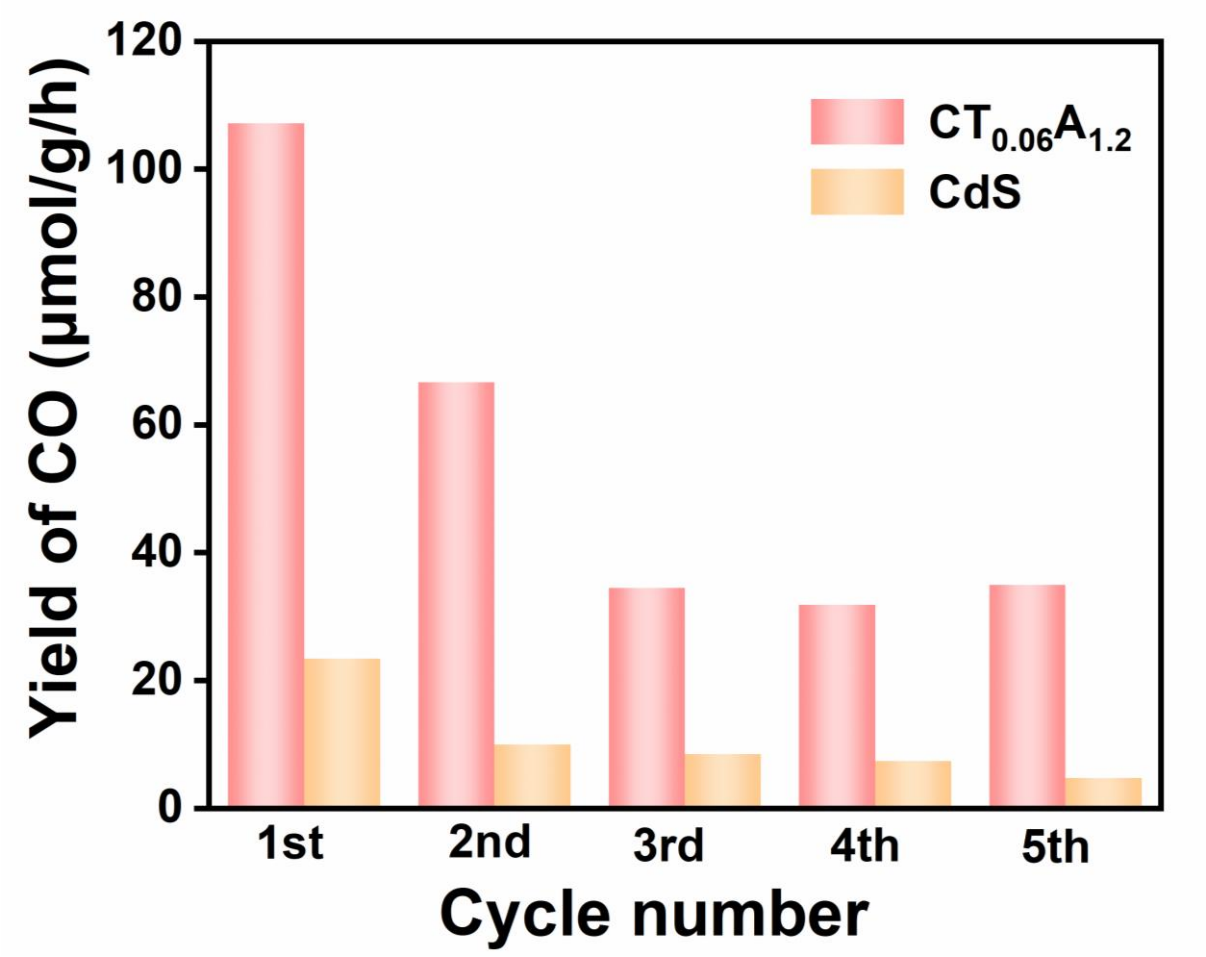

Fig. S10.Stability measurements for CdS and $CT_{0.06}A_{1.2}$.

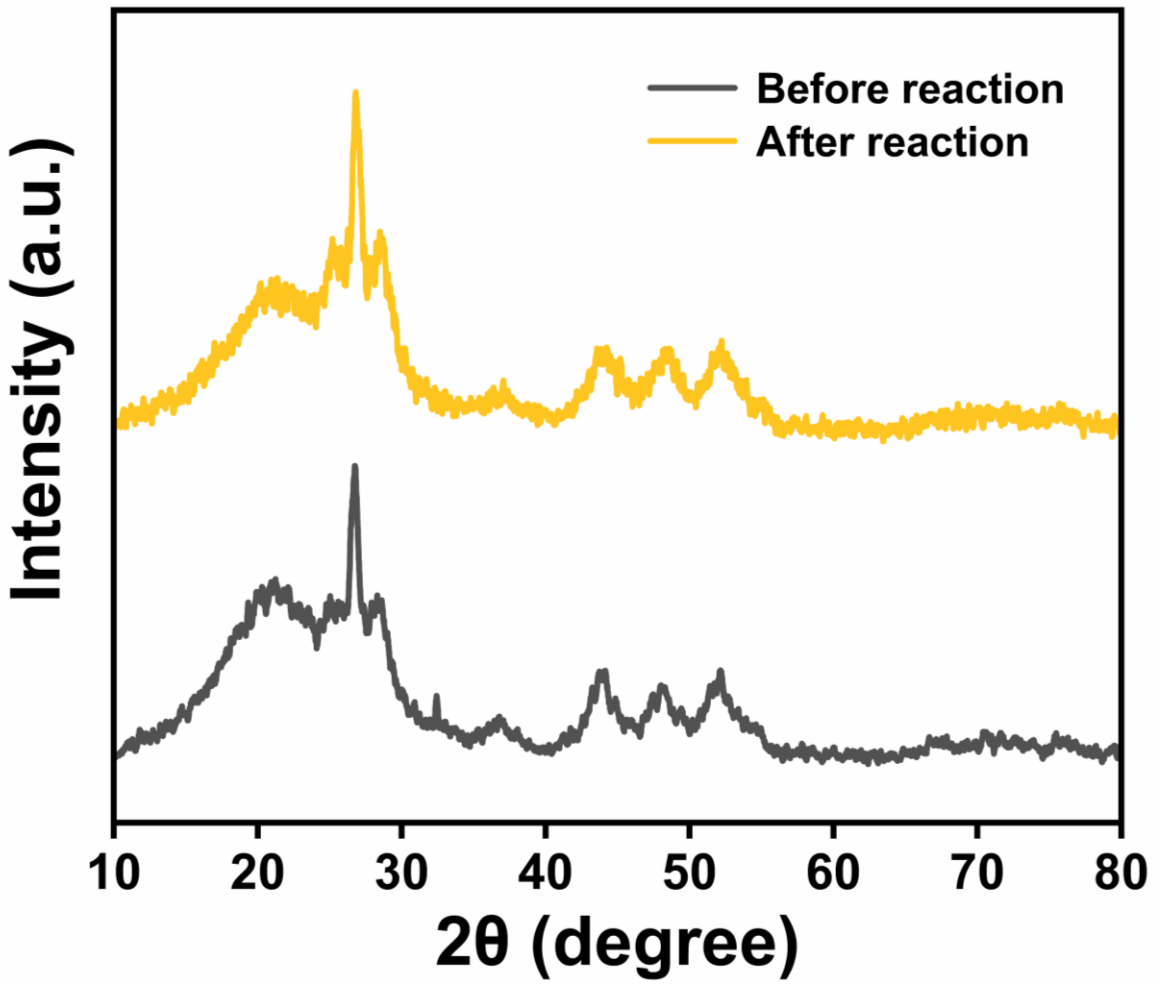

Fig. S11. XRD patterns of CTA before and after reaction.

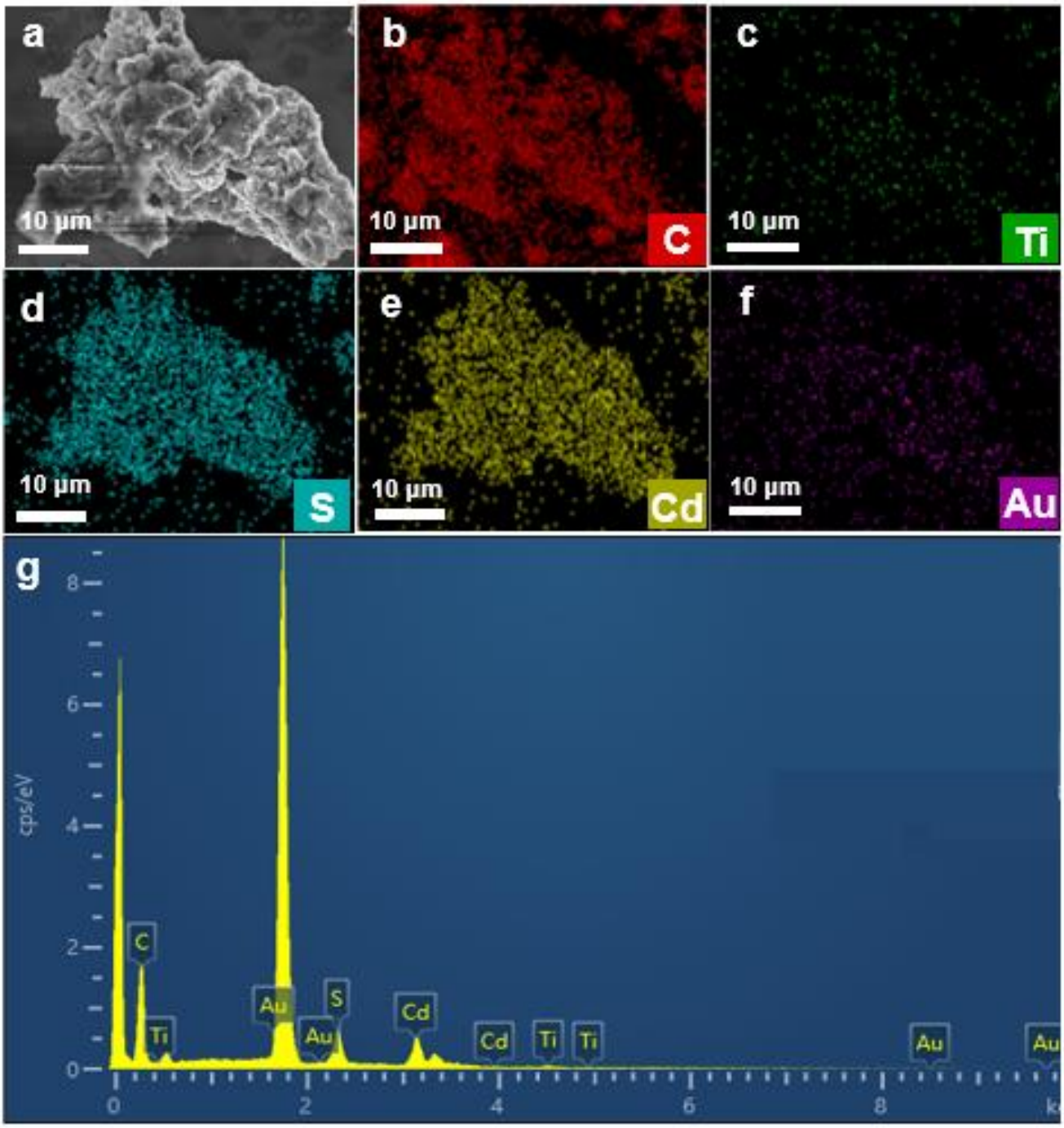

Fig. S12. (a) FESEM image of CTA after cyclic reaction with corresponding (b) EDS and (c-g) elemental mapping results.

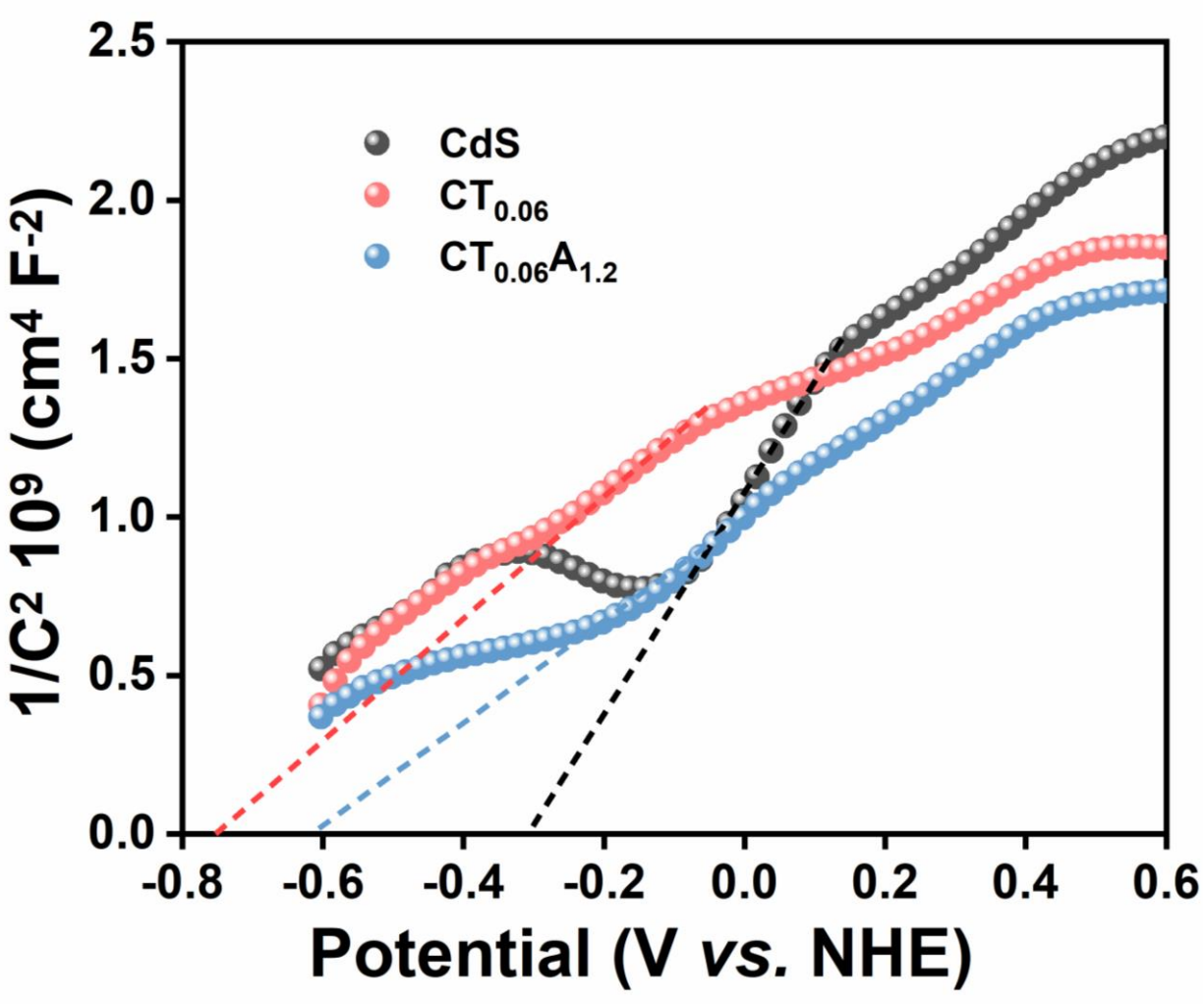

Fig. S13. (a) Mott−Schottky plots of CdS, $CT_{0.06}$ and $CT_{0.06}A_{1.2}$.

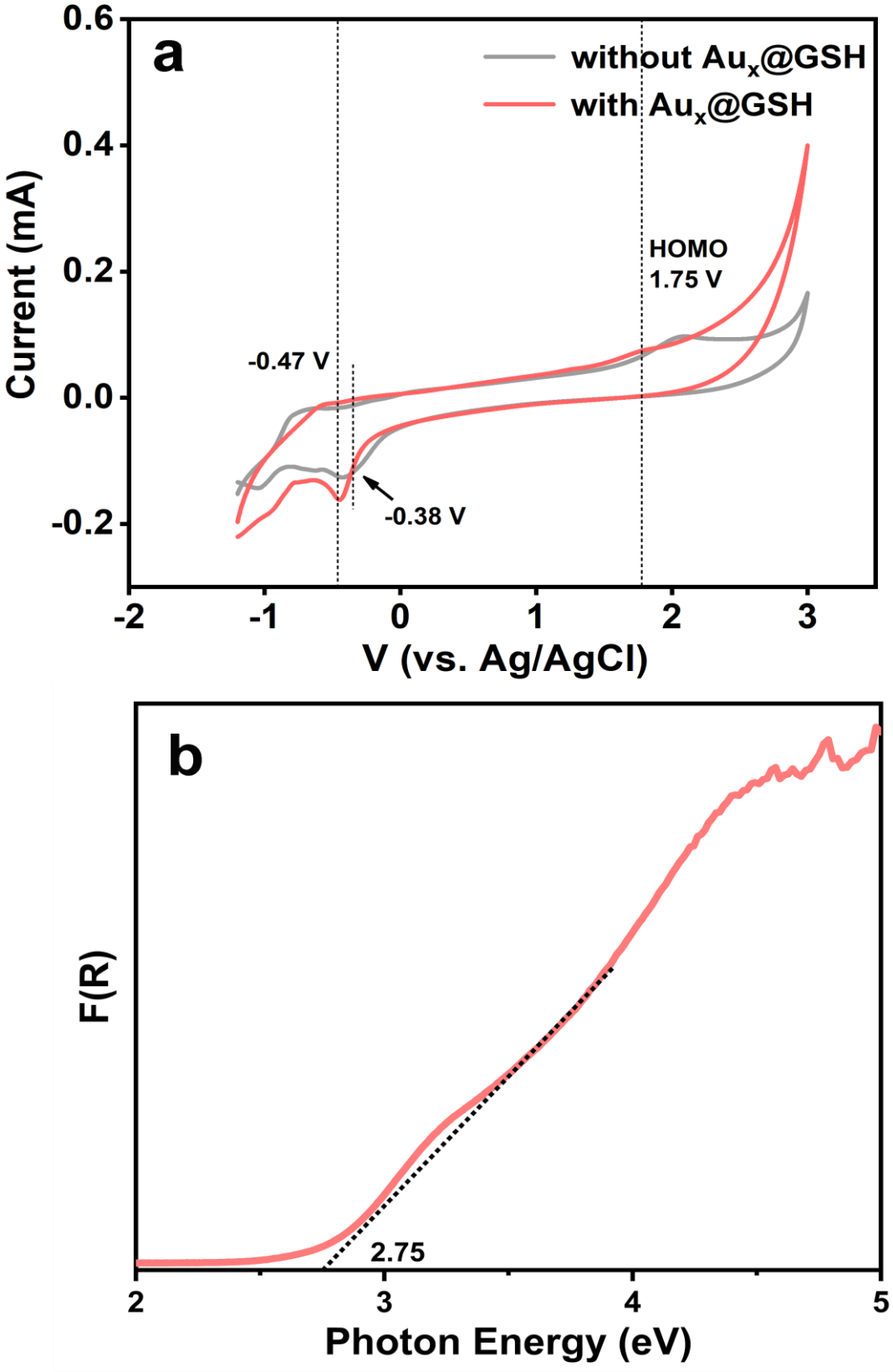

Fig S14. (a) CV curves of Au_x@GSH NCs. (electrolyte: degassed acetonitrile containing 0.1 mol L^{-1} TEAP); (b) Transformed plots based on the Kubelka−Munk function vs. the energy of light for Au_x@GSH NCs.

Table S1. Peak position with corresponding functional groups.

Peak position (cm^{-1})	**Vibrational mode**	**Reference**
2917/2856	υ_{-CH_2}	[4]
1630	δ_{-NH_2} & υ_{-OH}	[2]
3423	υ_{-COOH} & υ_{-NH_2}	[2]
613	Ti-O	[5]

Table S2. Summary of the specific surface area, pore volume and pore size of CdS, CT and CTA.

Samples	SBET (m^2g^{-1})[a]	Total pore volume(cm^3g^{-1})[b]	Average pore size (nm)[c]
CdS	36.0810	0.081219	9.00410
CT	67.7794	0.119111	7.02936
CTA	54.5328	0.109915	8.06232

a BET surface area is calculated from the linear part of BET plot.

b Single point total pore volume of the pores at P/P_0=0.95.

c Adsorption average pore width (4V/A by BET).

Table S3. Chemical bond species vs. B.E. for different samples.

Elements	CdS	CT	CTA	Chemical bond species	Reference
Cd $3d_{5/2}$	403.5	404.9	405	Cd^{2+}	[6]
Cd $3d_{3/2}$	410.3	411.7	411.8	Cd^{2+}	[6]
S $3d_{3/2}$	160.3	161.3	161.4	S^{2-}	[7]
S $3d_{1/2}$	161.9	162.4	162.6	S^{2-}	[7]
C 1s A	N.D.	284.8	284.8	C-C	[8]
C 1s B	N.D.	281.7	281.5	C-Ti	[8]
C 1s C	N.D.	286.2	286.2	C-O-C	[8]
C 1s D	N.D.	288.1	288.1	C-F	[8]
Ti 2p A	N.D.	458.7	N.D.	Ti-C	[6]
Ti 2p B	N.D.	460.2	N.D.	Ti-C	[6]
Ti 2p C	N.D.	463.1	N.D.	Ti-O	[6]
Ti 2p D	N.D.	462.2	N.D.	$Ti-O_x$	[6]
Ti 2p E	N.D.	455.5	N.D.	$Ti-O_x$	[6]
Ti 2p F	N.D.	461.0	N.D.	Ti-x	[6]
Au $4f_{5/2}$	N.D.	N.D.	88.2	Metallic Au^0	[9]
Au $4f_{5/2}$	N.D.	N.D.	89.0	Au^+	[9]
Au $4f_{7/2}$	N.D.	N.D.	84.5	Metallic Au^0	[9]
Au $4f_{7/2}$	N.D.	N.D.	85.4	Au^+	[9]

Table S4. Fitted EIS results of sample under visible light irradiation based on the equivalent circuit.

Photoandes	Rs/ohm	CPE/(×10^-5 F cm^{-2})	Rct/ohm
CdS	14.92	6.791	8869
CT	15.66	5.874	7190
CTA	14.74	7.448	5971

Reference

[1]X. Xie, N. Zhang, Z.-R. Tang, M. Anpo and Y.-J. Xu, $Ti_3C_2T_x$ MXene as a Janus cocatalyst for concurrent promoted photoactivity and inhibited photocorrosion, Appl. Catal. B-Environ. 237 (2018) 43-49.

[2]H. Liang, B.-J. Liu, B. Tang, S.-C. Zhu, S. Li, X.-Z. Ge, J.-L. Li, J.-R. Zhu and F.-X. Xiao, Atomically Precise Metal Nanocluster-Mediated Photocatalysis, ACS Catal. 12 (2022) 4216-4226.

[3]X.-Y. Fu, Z.-Q. Wei, S. Xu, X. Lin, S. Hou and F.-X. Xiao, Maneuvering Intrinsic Instability of Metal Nanoclusters for Boosted Solar-Powered Hydrogen Production, The Journal of Physical Chemistry Letters 11 (2020) 9138–9143.

[4]Q. Zhang, Q. An, X. Luan, H. Huang, X. Li, Z. Meng, W. Tong, X. Chen, P. K. Chu and Y. Zhang, Achieving significantly enhanced visible-light photocatalytic efficiency using a polyelectrolyte: the composites of exfoliated titania nanosheets, graphene, and poly(diallyl-dimethyl-ammonium chloride), Nanoscale 7 (2015) 14002-14009.

[5]X. Li, G. Fan and C. Zeng, Synthesis of ruthenium nanoparticles deposited on graphene-like transition metal carbide as an effective catalyst for the hydrolysis of sodium borohydride, Int. J. Hydrogen Energy. 39 (2014) 14927-14934.

[6]X. Chen, Y. Guo, R. Bian, Y. Ji, X. Wang, X. Zhang, H. Cui and J. Tian, Titanium carbide MXenes coupled with cadmium sulfide nanosheets as two-dimensional/two-dimensional heterostructures for photocatalytic hydrogen production, J. Colloid Interface Sci. 613 (2022) 644-651.

[7]M. N. Meeran, N. Haridharan, M. Shkir, H. Algarni and V. R. M. Reddy, Rationally designed 1D $CdS/TiO_2@Ti_3C_2$ multi-components nanocomposites for enhanced visible light photocatalytic hydrogen production, Chem. Phys. Lett. 809 (2022) 140150-140159.

[8]Y. Xia, B. Cheng, J. Fan, J. Yu and G. Liu, Unraveling Photoexcited Charge Transfer Pathway and Process of CdS/Graphene Nanoribbon Composites toward Visible-Light Photocatalytic Hydrogen Evolution, Small 15 (2019) 1902459-1902468.

[9]S. Hou, M.-H. Huang and F.-X. Xiao, Stabilizing atomically precise metal nanoclusters as simultaneous charge relay mediators and photosensitizers, J. Mater. Chem. A. 10 (2022) 7006-7012.